SUPPLEMNTARY NOTES

Comparison Plot

The progression of performance along the sampling trajectory is analyzed. The Figure S1, shows the comparison of how effectively each method utilizes its trajectory. Since DDPM, DDIM, and score-based sampling operate with different numbers of denoising steps (1000, 50, and 500, respectively), the performance is reported as a function of normalized reverse progress percentage rather than the step count. The results show that DDIM achieves faster early convergence, reaching higher PSNR in the initial stages. DDPM improves more gradually, requiring a longer trajectory to recover and achieve comparable performance. In contrast, the score-based method attains the highest final PSNR, with a sharp improvement in the later stages.

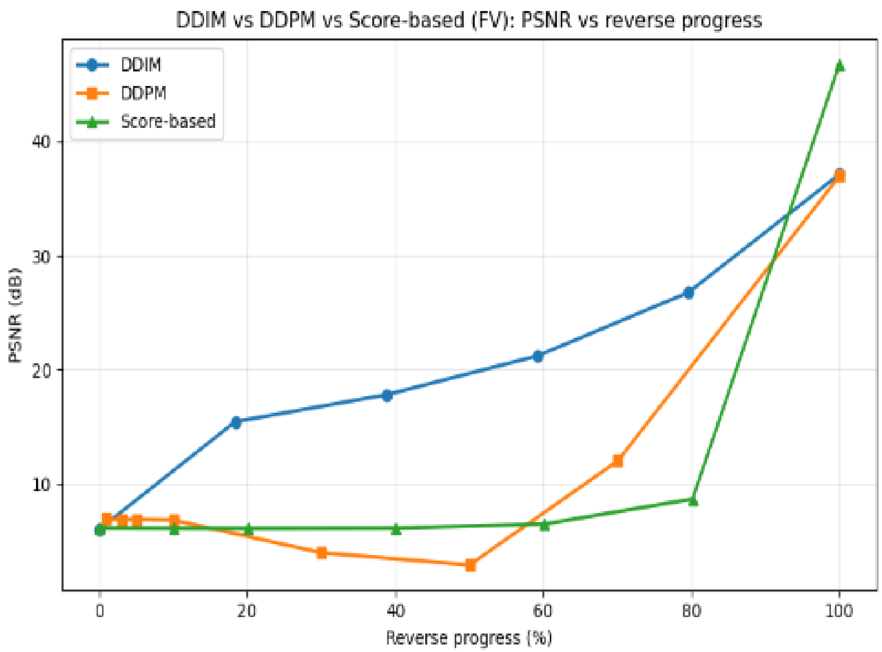

Supplementary Figure S1: Comparison of PSNR versus reverse progress percentage for DDPM, DDIM, and the score-based model.

Forward Operator Analysis

The forward operators corresponding to different angular coverage settings were analyzed using singular value–based metrics, including the maximum singular value (σ_{max}), minimum singular value (σ_{min}), condition number($\sigma_{max}/\sigma_{min}$), and effective rank. Here, σ_{max} represents the strongest measurable mode, σ_{min} captures the weakest (near-null) modes, the condition number characterizes worst-case instability, and the effective rank quantifies the number of meaningful measurement modes.

The full-view operator (A_FV) exhibits the best conditioning, with the largest σ_{min}, lowest condition number, and highest effective rank, indicating stable recovery with minimal information loss. In contrast, limited-view configurations are increasingly ill-posed, as reflected by faster singular value decay and reduced effective rank. While the effective rank increases monotonically with angular coverage, the condition number shows an overall decreasing trend. However, LV50 shows high conditioning number due to an extremely small σ_{min}, indicating the presence of near-null-space modes. The singular value decay plot in figure 2 S2 shows that LV50 retains more usable modes than LV30 but exhibits a sharper drop in the tail, while LV70 shows improved stability with a slower decay and higher σ_{min}.

Forward Operator	$\sigma_{\max}$	$\sigma_{\min}$	Condition Number	Effective Rank
FV	0.012218	1.783145e-06	6.852153e+03	7591.820591
A_LV70	0.011623	6.034406e-09	1.926094e+06	6275.222965
A_LV50	0.011168	2.306005e-13	4.840720e+10	5020.310553
A_LV30	0.010429	3.633171e-12	2.870343e+09	3151.807892

Supplementary Table S1: Singular value characteristics of the forward operator under full-view (FV) configuration.

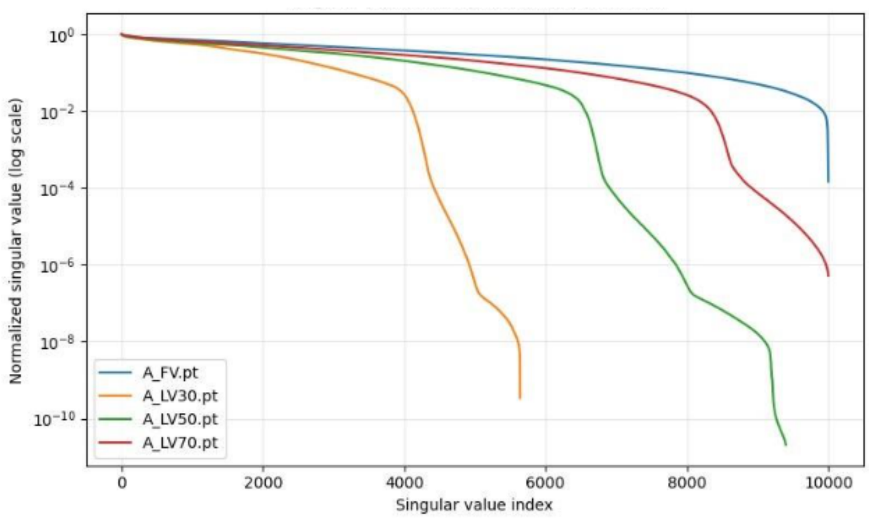

Supplementary Figure S2: Comparison plot of PSNR vs percentage of reverse progress of DDPM, DDIM, and Score Model

Noise level

The performance of the three models across varying noise levels was observed as in Figure S3. Each noise level is defined as a scaling factor on the variance of the clean measurement data, and the reported PSNR and SSIM values correspond to the mean over 100 test samples. The score-based model achieves high accuracy in low-noise settings, but as noise increases, the performance degrades rapidly, indicating more sensitivity to noise. DDPM and DDIM exhibit more gradual performance degradation, exhibiting more stable behaviour.

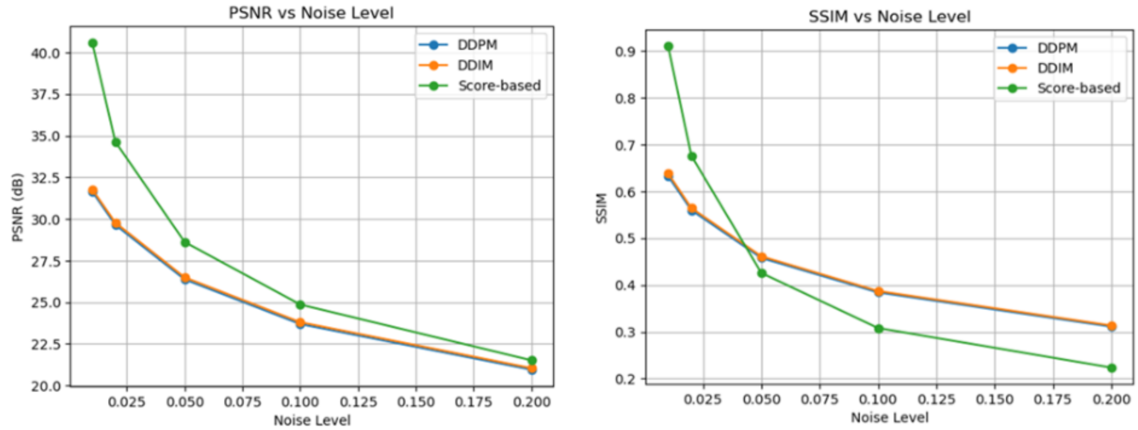

Supplementary Figure S3: PSNR and SSIM versus noise level for DDPM, DDIM, and score-based reconstruction methods.

Additional Coverage Performance

The limited view (LV) settings of 70%, 50%, and 30% detector coverage represents three practical cases of data availability: near-complete coverage (70%), moderately ill-posed acquisition (50%), and severely limited-view conditions (30%). As per the recommendation, an intermediate LV-40% setting was evaluated to further examine this transition. The results as summarized in Table S2 and S3, show a gradual degradation in performance with reduced coverage, while the refinement step consistently improves reconstruction quality across all settings, including LV-40%. The LV-40% results lie smoothly between the LV-50% and LV-30% cases, indicating that the performance trend can be reasonably interpolated between these setting. Additionally, the observed behaviour suggests a smooth transition in performance from LV-70 to LV-30, rather than a sharp inflection point. The score-based model maintains strong performance at higher coverage and shows a steady decline as coverage decreases. These findings indicate that the selected LV settings, including LV-40%, sufficiently capture the performance trends across varying acquisition conditions.

		DDPM					**DDIM**				
Model	Metric	FV	LV-70	LV-50	LV-40	LV-30	FV	LV-70	LV-50	LV-40	LV-30
Without refinement	PSNR	36.39	26.56	15.79	12.26	8.87	36.70	27.04	17.68	13.84	10.31
	SSIM	0.875	0.450	0.229	0.1488	0.073	0.898	0.487	0.265	0.1779	0.092
	LPIPS	0.021	0.222	0.436	0.5200	0.618	0.016	0.195	0.392	0.4718	0.563
With refinement	PSNR	36.95	34.27	29.08	21.98	17.29	37.10	34.57	29.74	20.75	16.05
	SSIM	0.925	0.828	0.575	0.4161	0.256	0.935	0.849	0.612	0.4323	0.268
	LPIPS	0.014	0.127	0.259	0.3431	0.464	0.012	0.114	0.237	0.3151	0.417

Supplementary Table S2: Reconstruction performance of DDPM and DDIM for 100 test samples under full-view and limited-view settings (70%, 50%, 40%, and 30%), reported with and without refinement.

Metric	FV	LV-70	LV-50	LV-40	LV-30
PSNR	46.75	45.73	40.87	30.29	23.75
SSIM	0.976	0.988	0.9889	0.9357	0.815
LPIPS	0.0006	0.0007	0.0019	0.017 88	0.077

Supplementary Table S3: Reconstruction performance of the score-based model for 100 test samples under full-view and limited-view settings (70%, 50%, 40%, and 30%).

Distribution plots

The histograms and boxplots are shown in Figures S4,S5, and S6 for DDPM, DDIM and score-based models respectively, capture the distribution of PSNR and SSIM across the 100 test samples, reflecting variability in reconstruction performance. These plots provide insight into the consistency and reliability of the reconstructions using different models for 100 samples.

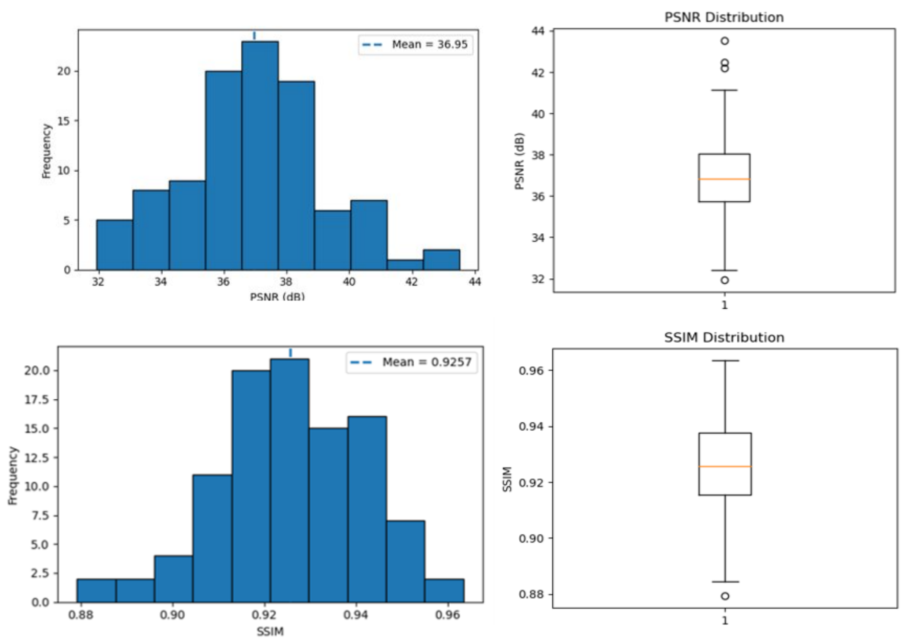

Supplementary Figure S4: Distribution of PSNR and SSIM for DDPM-based PAT reconstruction over 100 test samples.

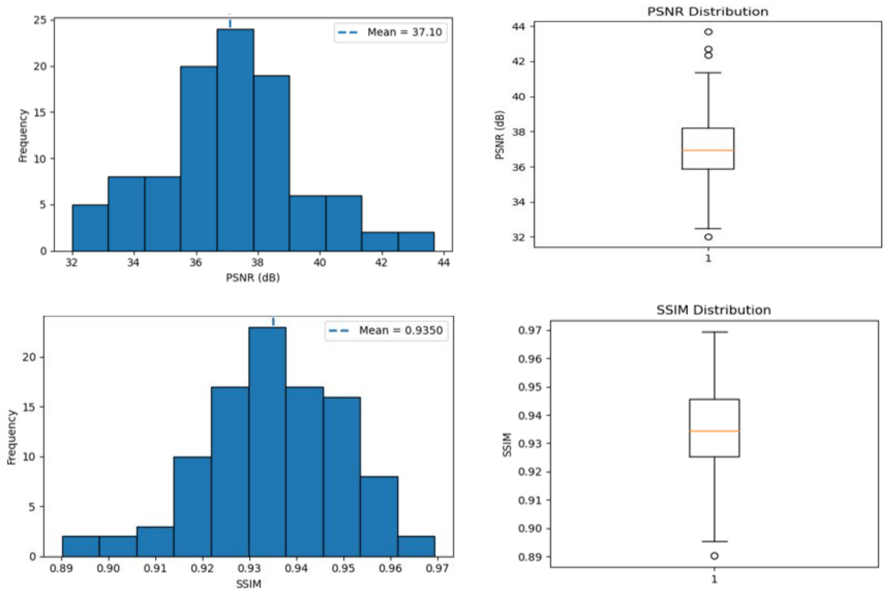

Supplementary Figure S5: Distribution of PSNR and SSIM for DDPM-based PAT reconstruction over 100 test samples.

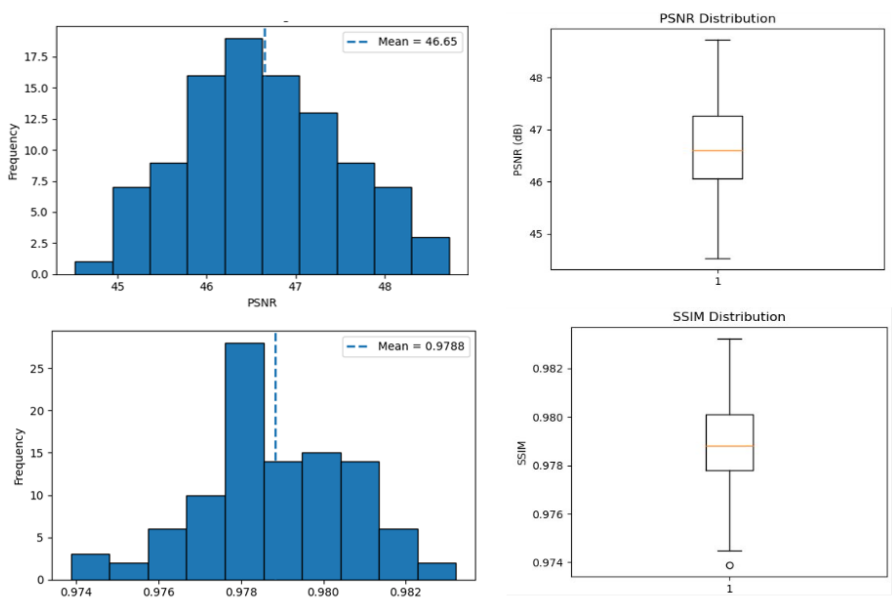

Supplementary Figure S6: Distribution of PSNR and SSIM for DDPM-based PAT reconstruction over 100 test samples.